SPACE TELESCOPE SCIENCE INSTITUTE
Operated for NASA by AURA

WFC3 Instrument Science Report 2015-15

Persistence in the WFC3 IR Detector: An Improved Model Incorporating the Effects of Exposure Time

Knox S. Long, Sylvia M. Baggett, & John W. MacKenty
September 21, 2015

ABSTRACT

Afterglows of earlier exposures, a phenomenon known as persistence, are seen in some images taken with the IR detector on WFC3. The amount of persistence is almost certainly a function of the complete exposure history of a pixel in the detector. However, the model currently being used to predict persistence in the IR channel of WFC3 depends solely on fluence associated with an earlier exposure and the time since that exposure. Here we describe the development of an improved model of persistence based on analysis of a set of observations of Omega Cen and 47 Tuc. We compare two similar parameterizations of persistence, both of which add the exposure time of the earlier exposure as an additional factor in the persistence prediction. We quantify the degree to which these two parameterizations improve our ability to predict persistence in WFC3 IR observations. The new parameterizations have been incorporated into the software package that is used to predict persistence in all WFC3 IR observations.

Introduction

Persistence is an afterimage of earlier exposures seen in IR detectors, including the HgCdTe IR detector on WFC3. It arises from defects within the detector diodes, which trap charge during the earlier exposure and release this charge slowly over time (See Smith et al. 2008ab). This charge being released is detected in subsequent exposures. Since charge is only released from pixels that were illuminated in the earlier source, an afterimage is created. Persistence is therefore an image anomaly which users need to consider when analyzing IR data from the WFC3, and other IR detectors.

Long et al. (2012) provided an initial description of persistence in the WFC3 detector based on several calibration programs in Cycles 17 and 18. Persistence is a strong

function of the fluence (the number of electrons released) of the source in the original image. For fluence levels less than half of full well, persistence is nearly always negligible in practical situations. However, for pixels that were saturated, the current due to persistence exceeds the dark current for several orbits.

Our initial model predicted persistence solely based on the fluence level in the initial exposure and the time since that exposure. If there was more than one earlier exposure that could have caused persistence, we also assumed that only the one that caused the most persistence contributed to the total persistence. The assumptions that went into this original model are in some sense equivalent to assuming that available traps are filled instantaneously.

Since 2012, STScI has used this model to estimate the amount of persistence in all WFC3 IR images, and made this information available to HST users through MAST (https://archive.stsci.edu/prepds/persist/search.php). The persistence predictions are useful primarily for identifying regions of the detector which are likely to be affected by persistence and therefore to be flagged as suspect for analysis. In certain situations, they may also be useful for removing persistence from images (See Long et al. 2012).

Since 2012, we have also carried out several sets of experiments intended to explore persistence in the WFC3 IR array in more detail. These experiments showed that the persistence depends not only on the fluence and the time delay, but also on the amount of time that a pixel remained filled with charge (Long et al. 2013ab). One simple qualitative interpretation of these results is that the traps that capture charge in the detector diodes have a distribution of trapping times as well as release times.

Here we report on a new set of observations that have allowed us to develop a more accurate prediction of persistence in the IR channel of WFC3, a prediction which takes into account, at least partially, the fact the trapping times are finite and comparable to typical exposure times. In this report, we consider only the spatially-averaged persistence; we discuss variations in persistence as a function of pixel position in a companion report (Long et al. 2015). Results derived from both reports have been incorporated into a new version (3.0.1) of the "persistence pipeline", the set of software tools used to estimate the persistence in all WFC3 IR images and to produce the persistence data products described above.

Observations and Reduction of the data

Calibration program 13572 consisted of single multi-accum exposure observations of 47 Tuc or portions of Omega Cen, hereafter the stimulus image, followed by a series of darks covering approximately 5000 s after the initial exposure. The stimulus image exposure times in the various visits ranged from 49 to 1403 s. Broadband filters were used in the visits with shorter exposures and narrow filters were used on the longer exposures in order to assure a wide range of fluence levels in all of the visits. Our choice of 47 Tuc for the shorter exposures was predicated on the fact that 47 Tuc contains stars of brighter apparent magnitude. The tradeoff in making this choice is that 47 Tuc is

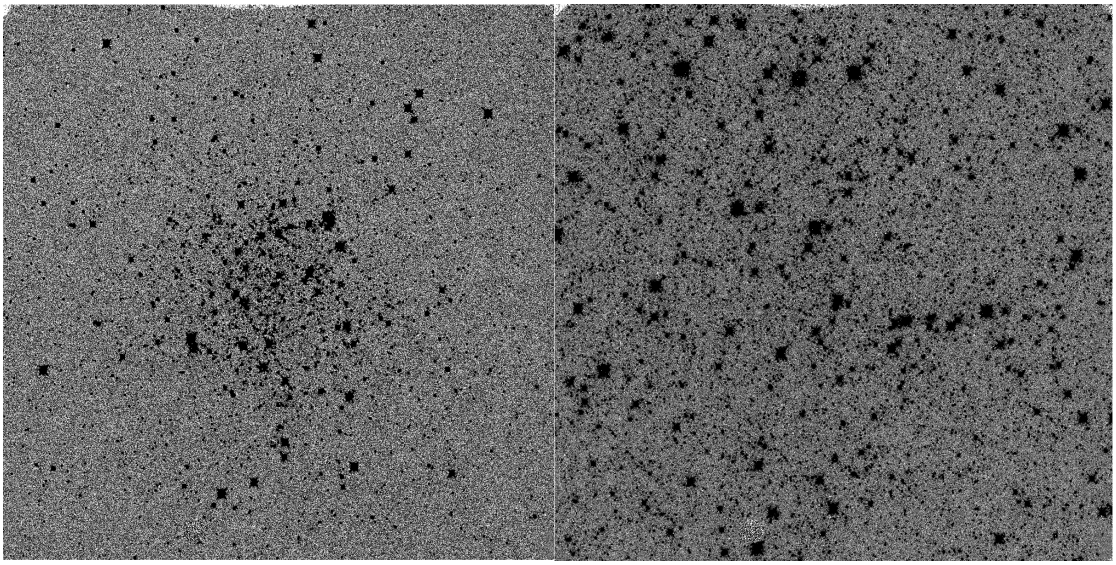

Figure 1. Persistence observed in dark exposures acquired approximately 1000 s after the 49 s and 1403 s exposures of 47 Tuc (left) and Omega Cen (right) in Visits 1 and 8, respectively. Both images, shown with an inverted colortable, are scaled linearly from -0.1 to 0.1 e s^{-1}.

Table 1. Observation Log

Visit	Dataset[a]	Obs Date	Target	Filter	Exp. (s)	Saturated[b] (%)
1	icgk01a8q	2013-11-18	NGC-104	F110W	49	6.1
5	icgk05hiq	2014-03-18	NGC-104	F110W	99	13.2
2	icgk02zpq	2014-03-06	NGC-104	F125W	149	11.9
6	icgk06ytq	2014-03-13	Omega Cen	F110W	199	9.2
3	icgk03jiq	2014-02-04	Omega Cen	F110W	499	25.9
7	icgk07wzq	2014-01-03	Omega Cen	F125W	799	25.3
4	icgk04eeq	2013-12-14	Omega Cen	F127M	1103	6.6
8	icgk08e2q	2014-02-10	Omega Cen	F127M	1403	8.7

[a] Dataset name associated with the external target exposure

[b] Percentage of pixels in the external exposure with a fluence level of at least 70,000 e, the nominal saturation level of the IR detector on WFC3.

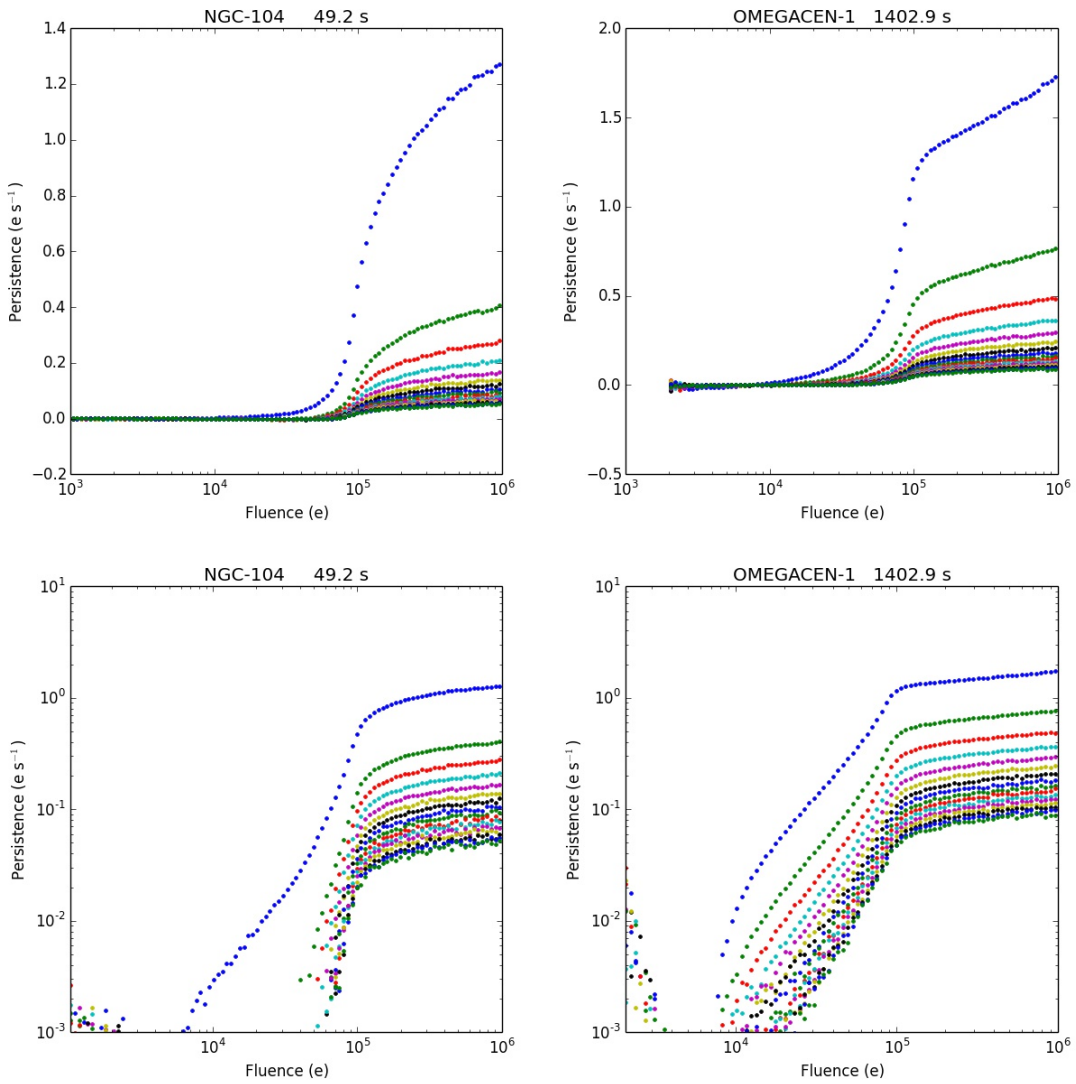

Figure 2. Two representations of the decay in persistence as a function of time after the 49 and 1403 s exposures of 47 Tuc (left) and Omega Cen (right) in Visits 1 and 8. The upper panels are log-linear representations of the decay while the the lower panels are log-log representations. Each curve shows the persistence measured in a dark as a function of the fluence in the 47 Tuc or Omega Cen exposure. For this 47 Tuc visit, the first dark was obtained 400 s after the end of the 47 Tuc exposures, and the last dark was obtained 6150 s afterward. For the Omega Cen visit shown the first dark shown was obtained 230 s after the Omega Cen exposure and the last about 3800 s afterward. Note the vertical scales in the upper panels differ; there is more persistence after the 1403 s exposure than the 49 s exposure.

much more compact than Omega Cen and therefore does not fill the detector's field of view as uniformly as Omega Cen. The observations are summarized in Table 1. The observational strategy is very similar to that used in Calibration Program 12694 in Cycle 19, except in that program we varied the number of exposures and not the exposure time (Long et al. 2013b). The persistence observed approximately 1000 s after the 49 and 1403 s exposures of 47 Tuc and Omega Cen is shown in Fig. 1.

To analyze the data, we first reprocessed all of the darks as if they were normal science observations, setting the header calibration keywords DARKCORR, ZSIGCORR, FLATCORR, and UNITCORR to PERFORM. In carrying out the reprocessing we used a dummy PFLTFILE with all values set to 1 (which applies the gain correction i.e. converts from units of DN to e). We then constructed the persistence curves for each of the darks from the "flt" files. These curves consist of the measured values in the individual DARK frames as a function of the fluence in the stimulus image. In constructing the curves, we eliminated any pixel that had poor data quality (flagged in the fits file data quality extension) in either the stimulus image or the dark.

The dark current in the WFC3 IR detector varies with time by 20 to 30% from its mean of 0.046 e s^{-1} for reasons that are not understood (Hilbert & Petro 2012). Since we want to measure persistence to as faint a level as possible, we have attempted to determine the dark current from each individual dark using regions that were not exposed to bright sources in the stimulus images. Specifically, we estimated the dark from all of the good pixels in regions of the detector with fluences less than 10,000 e in the stimulus images. Since this process uses the rates from one section of the detector to estimate background rates in other areas of the detector, we checked that the spatial variations in the dark were unlikely to affect our results by examining spatial variations in 61 darks from program 11929 with the same exposure times as the bulk of the darks taken as part of our calibration program. For these persistence-free darks we found the offset between the regions we used to measure persistence and the regions we used to measure background were negligible and the standard deviation of the errors were of order 0.003 e s^{-1}.

The persistence curves for Visits 1 and 8 (the same two visits shown previously in Fig. 1) are shown in Fig. 2 . Inspecting the semilog plots in the upper panels, we see that there is very little persistence ($\ll 0.05$ e s^{-1}) below a fluence of 30,000 e, especially beyond about 500 s after the end of the stimulus exposure. The log-log plots highlight clear differences in the shapes of the persistence curves. At fluence levels below about 70,000 e, persistence decays more rapidly after the 49 s exposure of 46 Tuc than it does after the long 1403 sec exposure of Omega Cen. Both sets of persistence curves show a "knee" at fluence levels of about 100,000 e, above which persistence rises more slowly. The break is undoubtedly related to the fact that the detector pixels saturate at about this point; the curves would look quite different if we had plotted the persistence as a function of the stimulus measured in raw pixel values (DN). However the break is much sharper in the persistence due to the longer exposure.

Though we have presented persistence curves for only the shortest and longest

stimulus exposures here, the trend based on all the datasets shows a gradual transformation in shape as one progresses from the shortest to the longest stimulus exposure times.

In Fig. 3, we show the decay of persistence due to different fluence levels as a function of time for the same two visits shown in Fig.1. Comparisons of the two panels of the figure show the same trends that had been seen in our earlier attempts to characterize persistence in the IR detector of WFC3:

1. Persistence decays roughly as a power law with time from an exposure at each fluence level,
2. The power law index is steeper at lower fluence levels,
3. At a given fluence level, the power law index is shallower for longer exposures
4. The amplitude of the persistence (at 1000 s) is higher for longer exposures.

A few other points are also worth noting. For the persistence following the 49 s stimulus exposure, there is a change in slope about 1000 s after the exposure. This is due to the fast decay of persistence at low fluence levels that we described earlier. In addition, as the figure shows, persistence measurements below about 0.01 e s^{-1} become quite noisy. Since approximately 1000 pixels are included in each curve, the difficulty in measuring very low levels of persistence is primarily due to the fact that it is difficult to accurately determine the the background level. All extracted persistence values from a given image contain the same background component (the features in one curve generally appear as features in the other curves) but the absolute background level fluctuates from image to image.

Analysis

As noted earlier, the model we are currently using to predict persistence is based solely on the degree of saturation in an exposure and on the time since that exposure took place. The functional form of our initial model, hereafter referred to as the "Fermi model", is as follows:

$$P_{ij} = A_{ij} \left(\frac{1}{e^{\frac{-(x-x_o)}{\delta x}} + 1} \right) \left(\frac{x}{x_o} \right)^{\alpha} \left(\frac{t}{1000\ s} \right)^{-\gamma}, \quad (1)$$

where P_{ij} is the persistence at time t after the end of an exposure with a fluence level of x. The first term A_{ij} in this equation describes a spatially dependent normalization, while the second term is a Fermi-like distribution that describes the rapid rise in persistence near saturation in terms of a characteristic fluence x_o and width δx. The third term in the equation describes a slow rise in persistence (generated by very high fluences) in terms of a power law with exponent α, while the fourth describes the decay with time in terms of a power law with exponent γ. If there are multiple exposures that could

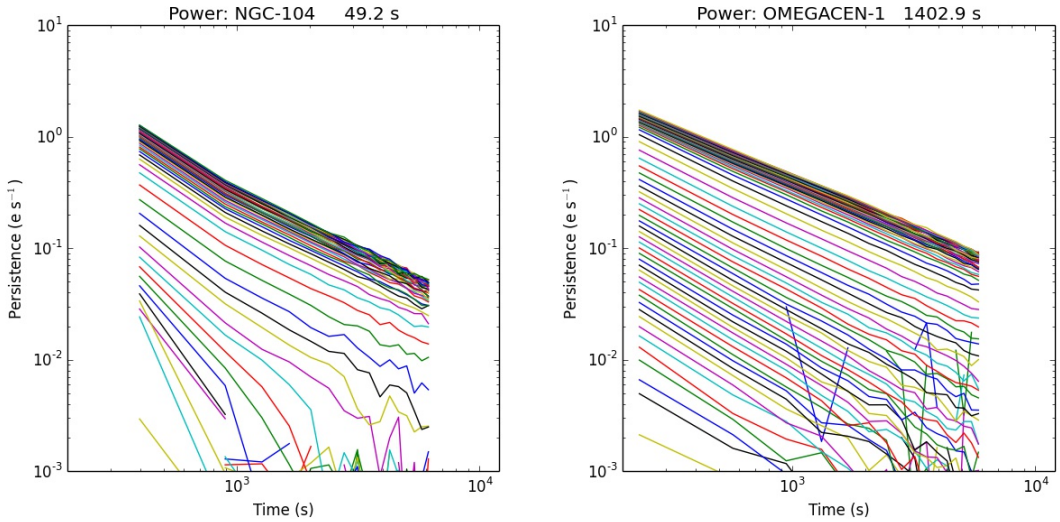

Figure 3. Persistence for different fluence levels as a function of time after the 49 s and 1403 s exposures of 47 Tuc (left) and Omega Cen (right)

cause persistence, the initial model counts only the exposure that would cause the most persistence in the current image.

There are a variety of ways that one could consider to improve our parameterization of the data. For example, one could conceive of a more physical model where as a pixel is filled with charge, more and more traps are exposed to free charge and each trap has a distribution of trap and release times that taken together duplicate the observed persistence. If such a model could be constructed (and we have experimented with such models), it could provide one with a great deal of insight into persistence as a phenomenon and allow predictions of persistence levels in a wide variety of situations. However, for this work, our goals are more modest, and therefore we have considered two simple extensions of our earlier phenomenological model.

In the first, the "exposure time dependent Fermi model", we simply fit the Fermi-like models to each of the visits and linearly interpolate the shape of the distribution at 1000 s and the power law decay constant for different exposure times.

In the second, the "exposure time dependent power law model", we simply carry out power law fits to each visit of the form

$$P = A\left(\frac{t}{1000\ s}\right)^{-\gamma} \tag{2}$$

where A and γ are functions of fluence and then interpolate on the basis of the exposure time to estimate the persistence in other observations. This approach has the advantage (in principle) that it does not impose a functional form on the shape of persistence and it allows for variations in the rate of decay as a function of the saturation level. If persistence were a separable function of fluence and time, then this might be expected

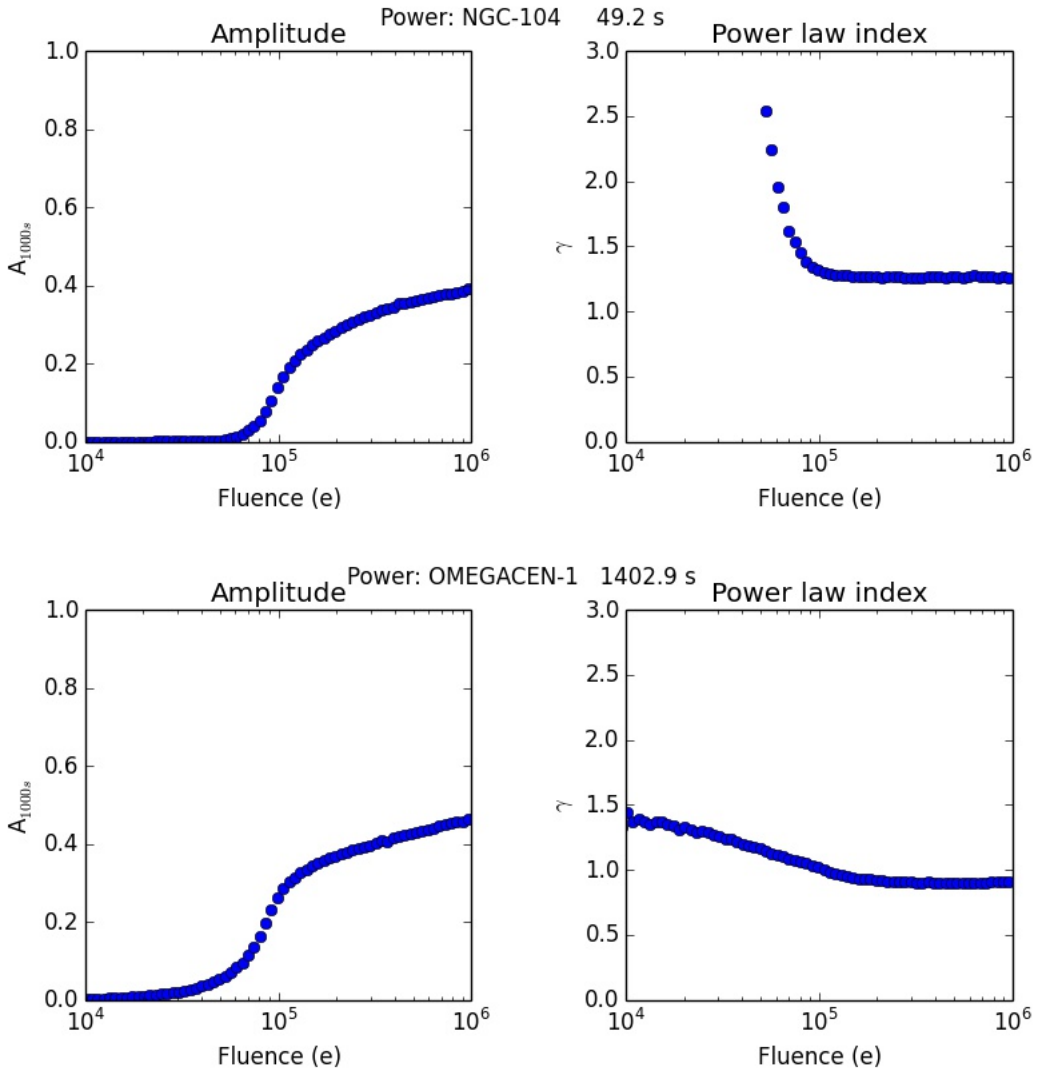

Figure 4. Results of fitting the simple power law model to persistence after the 49 and 1403 s exposures of 47 Tuc (top) and Omega Cen (bottom) .

Table 2. Parmeters of Fermi models for Various Exposure Times

Exp. (s)	A (e s^{-1}	x_o (e)	δx (e)	α	γ
49	0.251	97196	17346	0.206	1.269
99	0.282	96140	17889	0.197	1.232
149	0.280	91849	18067	0.187	1.096
199	0.287	90138	18612	0.178	1.078
499	0.317	83844	18909	0.146	1.005
799	0.323	78415	17547	0.141	0.964
1102	0.329	75202	17504	0.131	0.942
1402	0.328	73500	17755	0.126	0.921

to provide a better functional form for persistence than a model based on the previous functional form. Models of this type have a few disadvantages as well: (1) The power law model has many more free parameters since A and γ must be fit as functions of fluence, whereas in the Fermi-like model the fit contains only five free parameters. (2) The Fermi-like model provides a natural extension beyond the fluence level actually captured in the experiment, which the power-law fits do not.

The parameters derived from fitting the various visits to the Fermi-like model fits are shown in Table 2. These parameters reflect many of the basic characteristics of persistence as a function of the exposure time:

1. The amplitude parameter A increases with the length of the initial exposure.
2. The value of x_o decreases with exposure, reflecting the fact that even at low fluence levels there are some traps and these traps tend to have longer trapping times.
3. The value of α tends to increase with exposure time, reflecting the sharper "knee" in the persistence for longer exposures.
4. The value of γ decreases with time reflecting the fact that persistence last longer for longer exposure times.

Indeed the only parameter without an easy interpretation within the context of a model with finite trapping times is the width of the rise.

Examples of the results of power-law model fits to the data are shown in Fig. 4. They resemble in general terms the results that were described by Long et al. (2013b) for observations with an exposure time of 349 s, but now we have enough data to show how the fits vary with exposure time.

An important question is how well do our parameterizations actually describe the data. Visually, this is shown in Fig. 5 and Fig. 6 for the Fermi-model and power law models respectively. Not surprisingly the models are least accurate in an absolute sense at early times, when persistence is greatest. After about 1500 s, the Fermi-models tend

Table 3. Fitting Errors - Fermi-Like Model

Visit	Target	Exp. (s)	E1 (e s^{-1})	E2 (e s^{-1})	E3 (e s^{-1})	E4 (e s^{-1})	E5 (e s^{-1})	E6 (e s^{-1})
01	NGC-104	49	0.0022	0.0154	0.0271	0.0014	0.0046	0.0108
05	NGC-104	99	0.0029	0.0171	0.0248	0.0015	0.0042	0.0115
02	NGC-104	149	0.0044	0.0206	0.0146	0.0016	0.0038	0.0081
06	OMEGACEN-1	199	0.0052	0.0219	0.0138	0.0017	0.0037	0.0079
03	OMEGACEN-1	499	0.0075	0.0265	0.0090	0.0024	0.0068	0.0062
07	OMEGACEN-1	799	0.0088	0.0273	0.0077	0.0028	0.0090	0.0056
04	OMEGACEN-1	1103	0.0099	0.0275	0.0082	0.0025	0.0108	0.0054
08	OMEGACEN-1	1403	0.0103	0.0268	0.0087	0.0028	0.0116	0.0050

Table 4. Fitting Errors - Power Law Model

Visit	Target	Exp. (s)	E1 (e s^{-1})	E2 (e s^{-1})	E3 (e s^{-1})	E4 (e s^{-1})	E5 (e s^{-1})	E6 (e s^{-1})
1	NGC-104	49	0.0010	0.0076	0.0229	0.0008	0.0038	0.0102
5	NGC-104	99	0.0006	0.0086	0.0228	0.0010	0.0044	0.0107
2	NGC-104	149	0.0008	0.0059	0.0112	0.0008	0.0041	0.0068
6	OMEGACEN-1	199	0.0006	0.0064	0.0105	0.0008	0.0044	0.0063
3	OMEGACEN-1	499	0.0009	0.0058	0.0064	0.0010	0.0039	0.0031
7	OMEGACEN-1	799	0.0015	0.0052	0.0045	0.0015	0.0032	0.0020
4	OMEGACEN-1	1103	0.0006	0.0040	0.0038	0.0009	0.0024	0.0020
8	OMEGACEN-1	1403	0.0009	0.0037	0.0038	0.0011	0.0020	0.0019

to under-predict the persistence at high fluence levels by about 0.02 e s^{-1}, and over-predict the persistence in the region around 70,000 e. This is surely due to the fact that the Fermi-model prescription is by design less flexible than the power-law models.

For the power law fits, as shown in Fig. 6, the model also under-predicts the persistence at high fluence levels for visits in which the stimulus image has a short exposure time of 49 s, but for the longer exposure the errors are clearly smaller than for the Fermi-style models. If one inspects figures of the type shown in Fig 6 for other visits, one observes a gradual reduction in the amplitude of the features seen in the lower panels. At fluences greater than 10^5 e, the fact that the model underpredicts the data at late times is probably due to a the a fast decaying component at early times. The impact of this fast component is to steepen the power law index in the fit.

To provide a more quantitative measure of the accuracy of the model fits to the data, we have tabulated a "typical" error between the models and the data for 3 stimulus intervals and two time intervals following the initial exposure in Tables 3 and 4 for the Fermi and power law parameterizations of persistence . We define the mean error between the data and the model to be the average of the absolute value of the differences in a particular interval. We calculate the typical error for delay times less than 1500 s (E1, E2 and E3) and greater than 1500 s (E4, E5, and E6) so that we separate the time

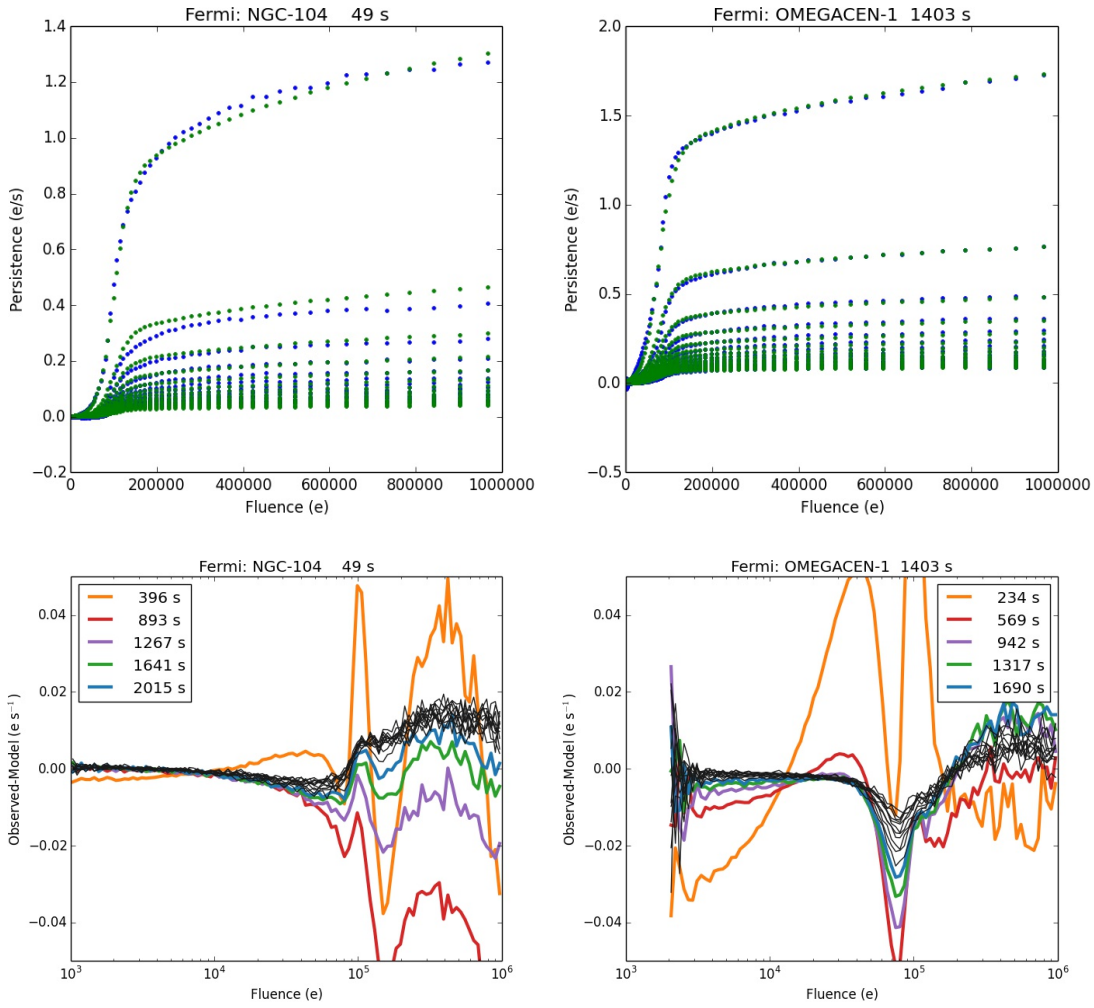

Figure 5. Fermi-model fits. The upper panels compare the observed persistence (blue) to the model fits (green) for the various darks obtained after the 49 and 1403 s exposures of 47 Tuc (left) and Omega Cen (right). The vertical scales in the upper panels are not identical; there is more persistence after the longer exposure. The lower panels show the difference between the measured persistence and the model. In these semi-log plots, the horizontal and vertical scales are the same.

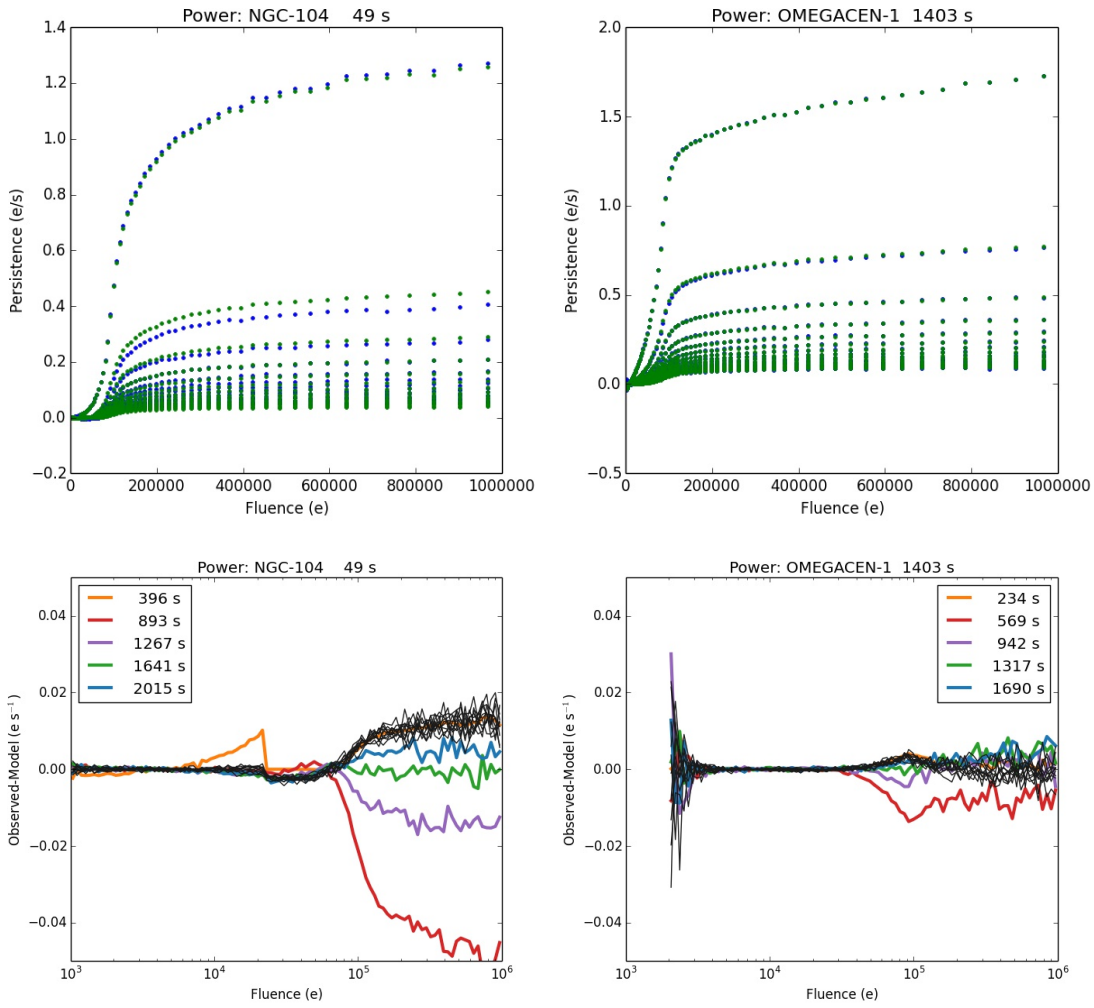

Figure 6. Power law fits. Plot format and scales are identical to those in Fig. 5. The errors in the model predictions are clearly smaller for the power law models than for the Fermi-like models.

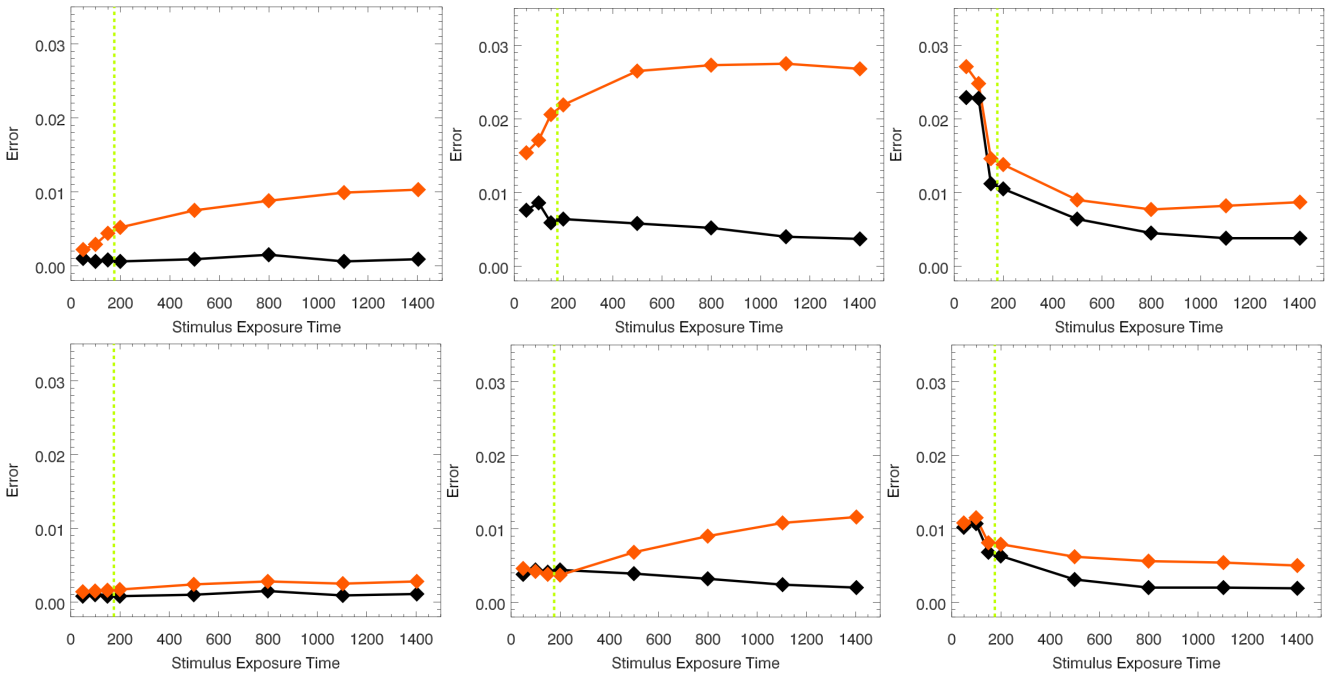

Figure 7. Error comparison. The Fermi model errors, in e s^{-1}, as a function of stimulus exposure time are shown in orange, the power law model errors in black. The top and bottom row of plots show results for data with delay times < 1500 s and > 1500 s, respectively. Stimulus levels in the plots from left to right are: $< 50,000$ e^{-1}, between $50,000 - 150,000$ e^{-1}, and $> 150,000$ e^{-1}. The light green vertical dashed line marks the switch between values measured from 47 Tuc (left of line) and Omega Cen (right of line). The typical dark rate is about 0.02 e s^{-1}.

delays that are likely to affect observations with a given orbit and those that are likely to affect later orbits (including orbits of other observers). Columns E1 and E4 correspond to the typical error for a stimulus below 50,000 e; columns E2 and E5 correspond to a stimulus between 50,000 e and 150,000 e, and Columns E3 and E6 correspond to a stimulus above 150,000 e. The error results are summarized graphically in Fig.7. Inspection of the errors confirms our impression from Fig. 5 and Fig. 6: the typical errors between the persistence model and the observed persistence are for the most part less than the typical dark rate (0.02 e s^{-1}), and often much less than this, especially for darks taken more than 1500 s after the stimulus exposure (E4, E5, and E6). This is partly due to the fact that the persistence is less at long times after the stimulus exposure, but also reflects the disappearance of short components to the persistence seen at early times. The tables and Fig.7 also show that the power law fits provide a better representation of the persistence in the calibration visits. The errors are usually smaller by a factor of 2 or 3. Focusing just on the power law parameterization, we see that the errors are typically 4 or 5x below the dark count rate in the first 1500 s after the exposure, and 5 to 10x below the dark rate at times greater than 1500 s.

The exposure-time dependent Fermi model and the exposure-time dependent power law models both represent an improvement over the original Fermi model described by Long et al. (2012). Both models have have been incorporated into the software package that is used to estimate persistence in all WFC3 IR observations (Version 3.0.1).[1] It is important to note, however, that at present we have calibration data only for the 8 exposure times listed in Table 1. We currently rely on linear interpolation for other exposure times, and so errors may be worse than indicated here. Additional observations with different exposures times are being carried out, and once these data are analyzed the associated calibration reference files will be updated.

Spatial Variations

As noted earlier, for the analysis described here we have treated the persistence in the IR channel of WFC3 as if it were uniform across the detector. That is not the case, however, as is discussed in a companion ISR (Long et al. 2015). For a given stimulus, persistence is about 20% higher in quadrant 1 (upper left) than in quadrant 4 (lower right). The spatial variations appear (to zeroth order) to be variations associated with the amplitude of the persistence and not associated with the duration of the persistence signal. If this is the case, then one can allow for spatial variations with a " correction flat". Effectively, this means the amplitude variable A in equations 1 and 2 is not simply a function of the fluence and the length of the exposure, but also has a position dependence. The correction flat is a standard part of our persistence model.

How Good is the Persistence Correction?

Determining how effective the persistence model is for estimating persistence in normal science observations is not straightforward, because one cannot easily measure the persistence in a typical observation, which is typically dominated by real objects in the current exposure[2].

We have, however, conducted a few experiments where we were able to attach a series of darks to IR exposures from other calibration programs. The most extensive experiment of this type was carried out as part of program 13173. The purpose of the program was to update the calibration of the FGS, but the UV observations that constituted the main program were sufficiently short that we were able to add a 703 s IR exposure and a series of darks to 15 of the visits. An example of the data obtained and of the quality of the persistence subtraction is shown in Fig. 8. The right-most image is the persistence-subtracted flt file from the first dark obtained after the stimulus

[1] In producing data products for MAST, we currently use the power law parameterization of persistence. However, with the appropriate command line switches, either the Fermi or the original parameterization of the persistence used in Version 2.1 can still be run.

[2] This statement is not entirely true for well-dithered observations. One can, in well-dithered observations, construct an image that is persistence-free, project this back into the frame of the original flt files and look for differences in the two images

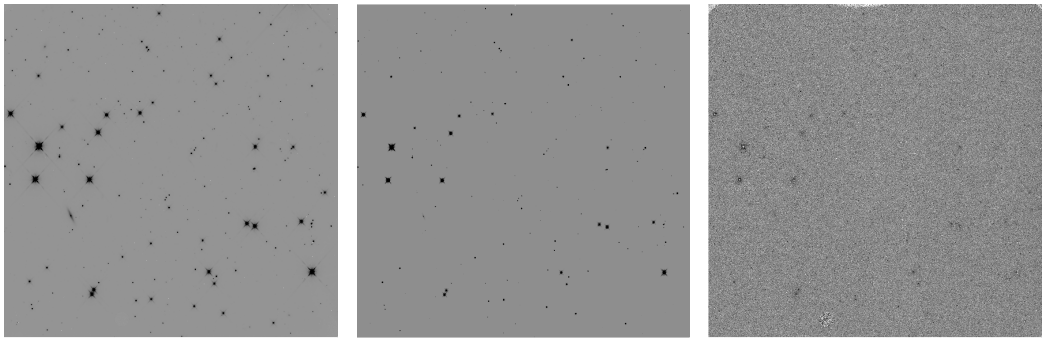

Figure 8. An example of the images obtained as part of Visit AC of program 13173. The first panel shows the external exposure of M35, scaled so the so that the darkest pixels have fluences of greater than 35,000 electrons, or half of saturation. The second shows the predicted persistence for the first dark after the M35 exposure with darkest pixels having a predicted persistence of greater than 0.5 e. The third panel shows the persistence-subtracted image with the same stretch as that of the persistence image. Most, but not all of the persistence has been removed.

exposure. Much of the persistence has been removed, but not all, as is evident from the faint smudges in the image shown in the third panel.

A more systematic estimate of the errors in the persistence model is shown in Fig. 9 for pixels that were saturated between 1×10^5 and 5×10^6 e, where saturation is nominally 7×10^4 e. In most but not all cases, 80 to 90% of the persistence is being subtracted, and most but not all of the time the residual persistence is less 0.04 e s^{-1}. Clearly, the model is under-estimating the persistence at delay times less than 1000 s. This is most probably a limitation due to the linear interpolation necessary between persistence curves obtained at exposure times of 499 and 799 s. In addition, there are also variations in results despite the fact that we are analyzing 15 identical visits. These are either variations due to our analysis process, which seems a bit unlikely, or the fact that the persistence affects different pixels in different visits, or most probably, intrinsic differences in persistence as a function of some parameter of the system which we do not understand. The results suggest that one should use the persistence model primarily as an indicator of which pixels to flag as having data quality issues, and that one should use the persistence-corrected flt files with great care.

A New Version of MAST Persistence Products

As noted earlier, STScI provides data products though MAST that allow observers to assess which portions of an image have been affected by persistence from earlier exposures. The algorithm used to date (Version 2.1 of the persistence software) is the Fermi-model described by Long et al. (2012), which did not allow for differences in

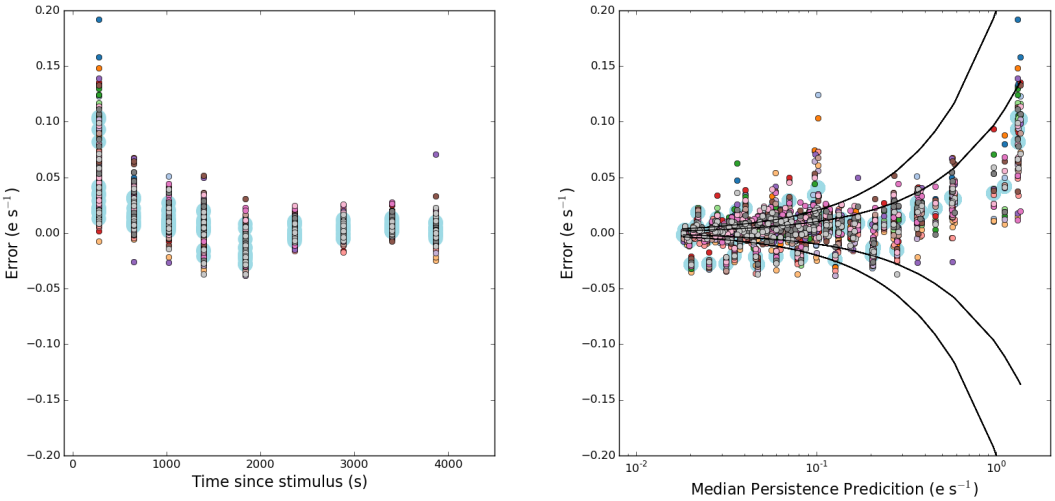

Figure 9. Left: The residual persistence measured as a function of time since stimulus for pixels which had a a fluence between between 1×10^5 and 5×10^6 e for all of the 15 visits. The light blue larger circles are the average error and the smaller circles represent measurements for 16 (4 x 4) subsections of the detector. Right: The error in the persistence subtraction as a function of the median persistence estimated from the model. The solid black lines show the envelopes for having removed 80 and 90% of the persistence. Some of the scatter at low levels of persistence (long times since the external exposure) likely reflect measurement errors .

persistence as a function of exposure time.[3] As of April 2015, all new data are being processed using the new power law model (Version 3.0.1 of the persistence software), based on the data described here and using the "correction flat" described by Long et al. 2015. Re-processing of all of the archival data is also underway.[4]

Summary and Conclusions

Here we have described a new model of persistence that takes into account variations in exposure time. Two versions of the new model exist. The first, the "exposure time dependent Fermi model", assumes a Fermi-like parameterization of the amplitude of persistence and a single power law decay exponent for each exposure time. The second, the "exposure time dependent power law model" uses a variable power law decay model for each exposure time. In both cases, interpolation is used to estimate the persistence when calibration data of a given exposure time is absent. Both models are an improvement over the original "Fermi model", but the exposure time dependent power law model matches the data better. Both still have limitations, in part because we do not yet have enough calibration data to avoid linear interpolation, and also in part because spatial variations in persistence are not fully understood (See Long et al. 2015). Nevertheless, as of April 2015, the "time dependent power law" parameterization for persistence is now being used in Version 3.0.1 of the "persistence pipeline" software to create data products available in MAST for users to assess the amount of persistence in their images.[5] Reprocessing to produce new estimates of persistence in all WFC3 IR data is also underway.

The next steps in understanding persistence involve obtaining a sufficient amount of data to test how repeatable persistence is in "identical situations" and to reduce the effects of interpolation on the existing parameterization. This is the subject of the Cycle 22 Calibration program.

Acknowledgments

We thank George Chapman, Merle Reinhart, Alan Welty, and Bill Januszewski for their help in crafting and executing this calibration program, Ariel Bowers, Heather Gunning and Harish Khandrika for their efforts in installing and running the persistence software on WFC3 IR data, and Gabriel Brammer for a careful reading of this manuscript.

[3] Version 2.1 did include a correction flat.

[4] As of Version 3.0.1 software, the version number is reported near the beginning of in html summary that is produced for each exposure. If this is missing, then this particular file has yet to be reprocessed.

[5] The "exposure time-dependent Fermi model" as well as the original "Fermi" model are still supported.

References

Long, K.S., Baggett S. M. & MacKenty, J. W. , 2013a, "Characterizing Persistence in the WFC3 IR Channel: Finite Trapping Times," WFC3 ISR 2013-06

Long, K.S., Baggett S. M. & MacKenty, J. W. , 2013b, "Characterizing Persistence in the WFC3 IR Channel: Observations of Omega Cen", WFC3 ISR 2013-07

Long, K.S., Baggett, S.M., MacKenty, J.W., and Riess, A.G., 2012, "Characterizing persistence in the IR detector within the Wide Field Camera 3 instrument on the Hubble Space Telescope," Proceedings of the SPIE, 8442, 84421W-9

Long, K. S., Baggett, S. M., MacKenty J. W. 2015, "Persistence in the WFC3 IR detector: Spatial Variations", ISR-2015-16

Smith, R.M., Zavodny, M., Rahmer, G. & Bonati, M., 2008a, "A theory for image persistence in HgCdTe photodiodes," Proceedings of the SPIE, 7021, 70210J-1

Smith, R. M., Zavodny, M., Rahmer, G., Bonati, M., 2008b, "Calibration of image persistence in HgCdTe photodiodes," Proceedings of the SPIE, 7021, 70210K-1